Supplemental Information for Graham et al.

.

Supplemental Figure 1

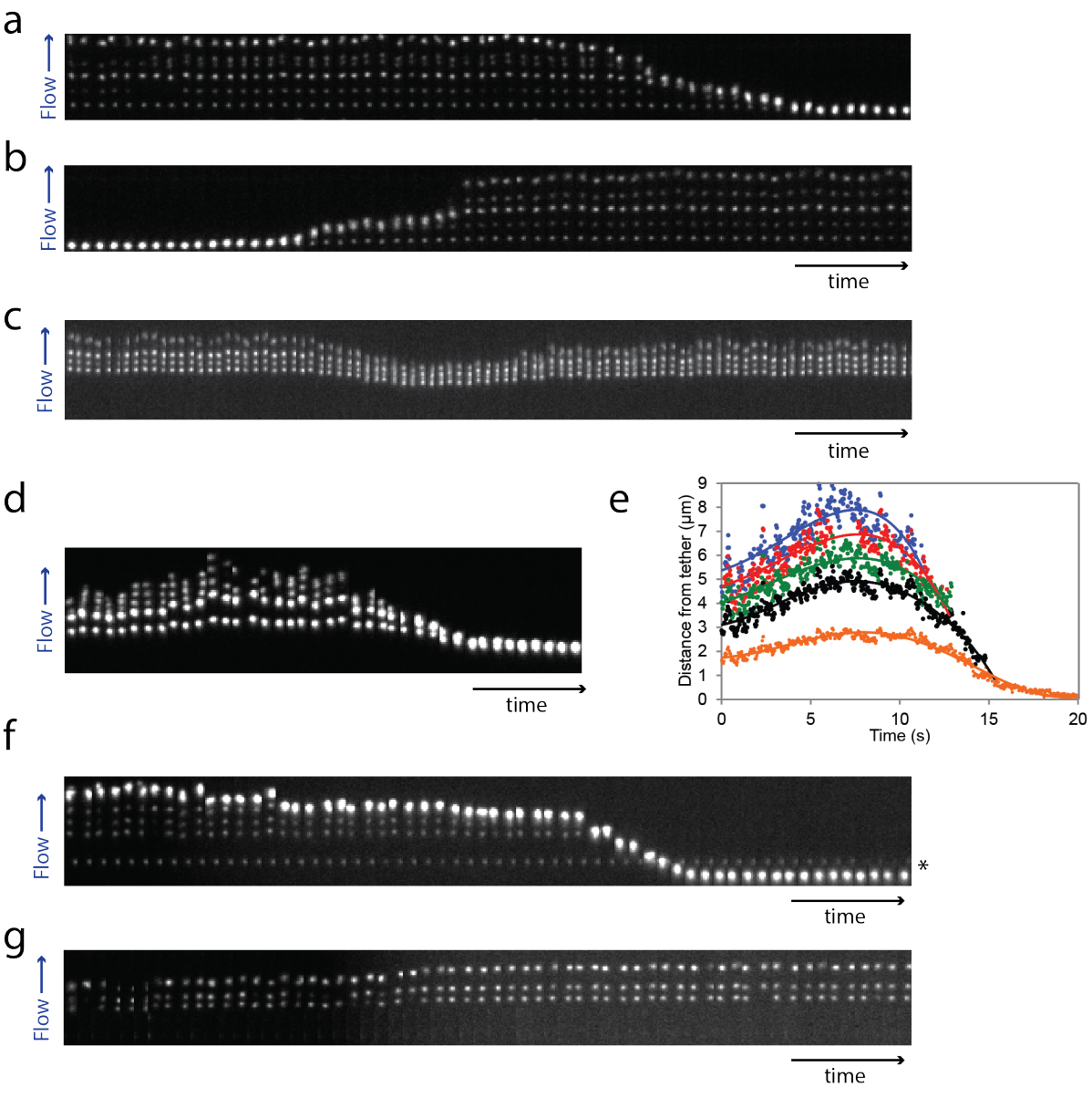

Supplemental Figure 1: Additional single-molecule compaction and decompaction results. (a) Montage showing compaction of λ DNA by 100 nM Spo0J protein in buffer containing 20 mM Tris pH 7.5, 100 mM NaCl, and 100 μg/ml BSA (1 s/frame). Note: In some cases, like this one, we observed EcoRI-QDs that bound stably at positions not predicted to be EcoRI sites. (b) Rapid decompaction upon washing with the same buffer containing 200 mM NaCl (100 ms/frame). (c) Montage showing transient compaction and subsequent decompaction by 720 nM HBsu in 20 mM HEPES-NaOH pH 7.5, 40 mM NaCl (600 ms/frame). Initial binding of HBsu compacts DNA by introducing local bends, while continued binding of HBsu leads to the formation of an extended filament on DNA, consistent with previous observations for *E. coli* HU (van Noort et al. 2004). (d) Compaction by 100 nM Spo0J + 10 nM HBsu of DNA pre-compacted with 10 nM HBsu in 20 mM Tris, pH 7.5, 100 mM NaCl, 100 μg/ml BSA (0.5 s/frame). Slight decompaction, likely due to partial displacement of HBsu by Spo0J, is followed by global compaction of the DNA to the tether point. (e) Vertical position over time of quantum dots in (d) obtained by 2-dimensional Gaussian fitting. For clarity, different quantum dots are color-coded. Lines are polynomial fits to the data and are intended solely to guide the eye. (f) A 1 s/frame montage of compaction by 500 nM H6-tagged H-NS in 20 mM Tris, pH 7.5, 50 mM NaCl, 10 mM $MgCl_2$, 100 μg/ml BSA. H-NS, which is known to bridge DNA under these buffer conditions, compacts DNA in an end-biased manner similar to Spo0J. A small concentration (5 nM) of rhodamine G tracer dye is responsible for the increase in background fluorescence upon arrival of the protein in the flowcell. The asterisk on the right indicates a stationary quantum dot bound nonspecifically to the surface. (g) Extension of DNA by 500 nM H-NS-H6 in 20 mM Tris, pH 7.5, 5 mM NaCl, 100 μg/ml BSA (1 s/frame), conditions that suppress the DNA bridging activity of H-NS and favor the formation of an extended nucleoprotein filament. As in (f), the increase in background fluorescence due to a tracer dye indicates arrival of the protein in the flowcell. The DNA is partially labeled with only 3 QDs in this montage.

Supplemental Figure 2

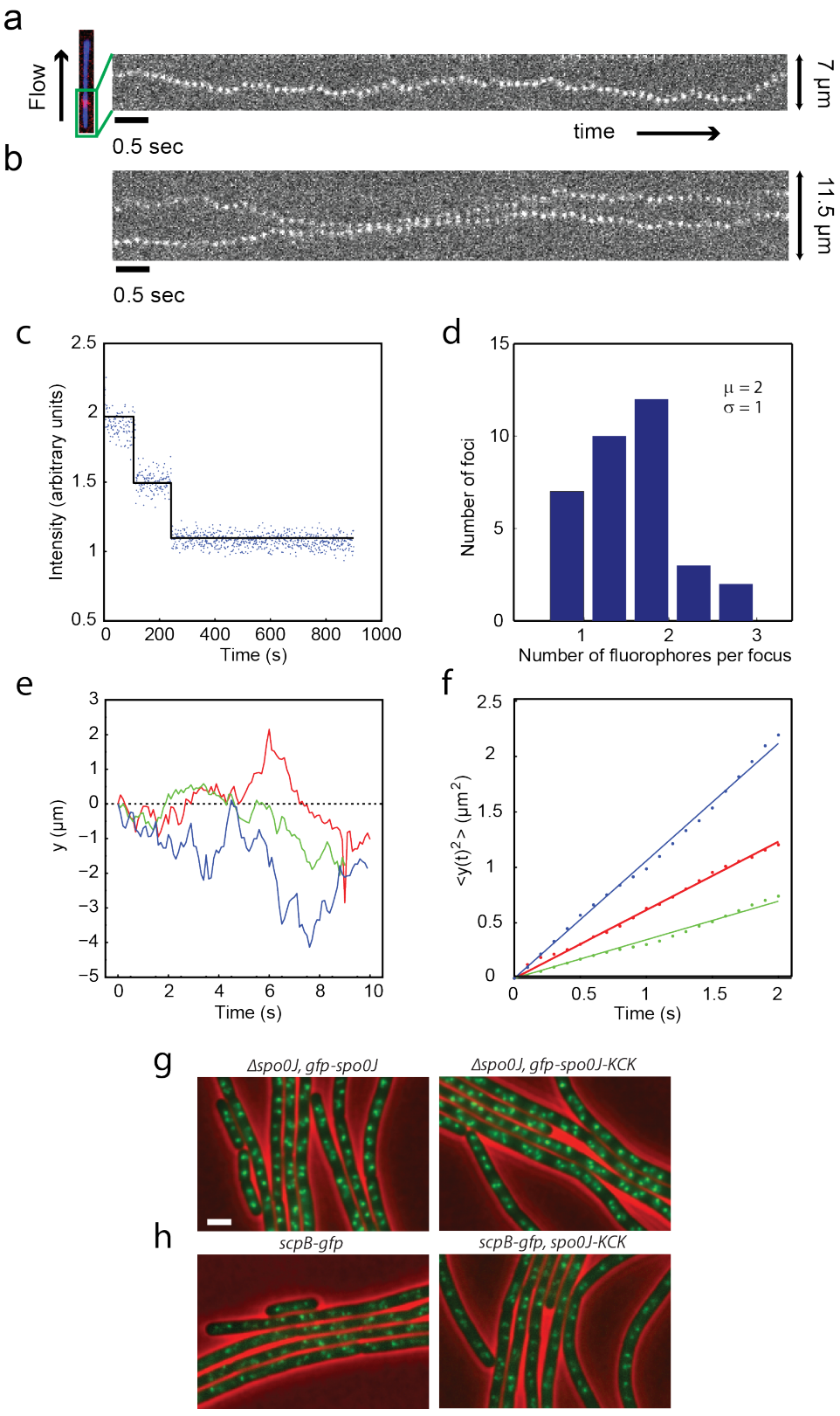

Supplemental Figure 2: Labeled Spo0J slides on DNA by 1-dimensional Brownian diffusion. (a-b) Individual kymographs showing sliding of labeled Spo0J on DNA. Pairs of Spo0J foci occasionally appeared to collide without associating (b). (c-d) Calibration of the intensity of individual Spo0J spots. Photobleaching of non-specifically bound Spo0J-Cy3 proteins on the surface of a glass coverslip was imaged with the same exposure time (100 ms) used to image sliding of Spo0J on DNA. (c) Traces of integrated intensity (arbitrary units) that showed obvious photobleaching steps (>100) were manually fitted with a step function. The size of each photobleaching step corresponds to the fluorescent intensity of a single fluorophore, which was then used to calibrate the integrated fluorescent intensity (background subtracted) of a sliding Spo0J focus. (d) Distribution of the calculated number of fluorophores per sliding Spo0J focus with an average of two fluorophores per focus. This suggested that sliding Spo0J foci were mainly dimeric. (e) Fitted one-dimensional diffusion trajectories of individual Cy3-labled Spo0J particles on flow-stretched DNA. (f) Mean-squared displacement plots of diffusion from the trajectories shown in (e). Spo0J dimers had an average diffusion constant of $3.0 \pm 1.9 \times 10^6$ bp^2/s, similar to observed values for other site-specific DNA binding proteins (Tafvizi et al. 2008; Blainey et al. 2006). (g) GFP-Spo0J-KCK (right panel) forms foci that are indistinguishable from GFP-Spo0J (left panel). (h) ScpB-GFP foci in cells expressing Spo0J-KCK (right panel) are similar to those in cells expressing wild-type Spo0J (left panel). GFP signal was pseudocolored green and phase contrast was pseudocolored red. The fluorescence signal in different images in (h) or (g) was adjusted to the same scale. Scale bar is 2 μm.

Supplemental Figure 3

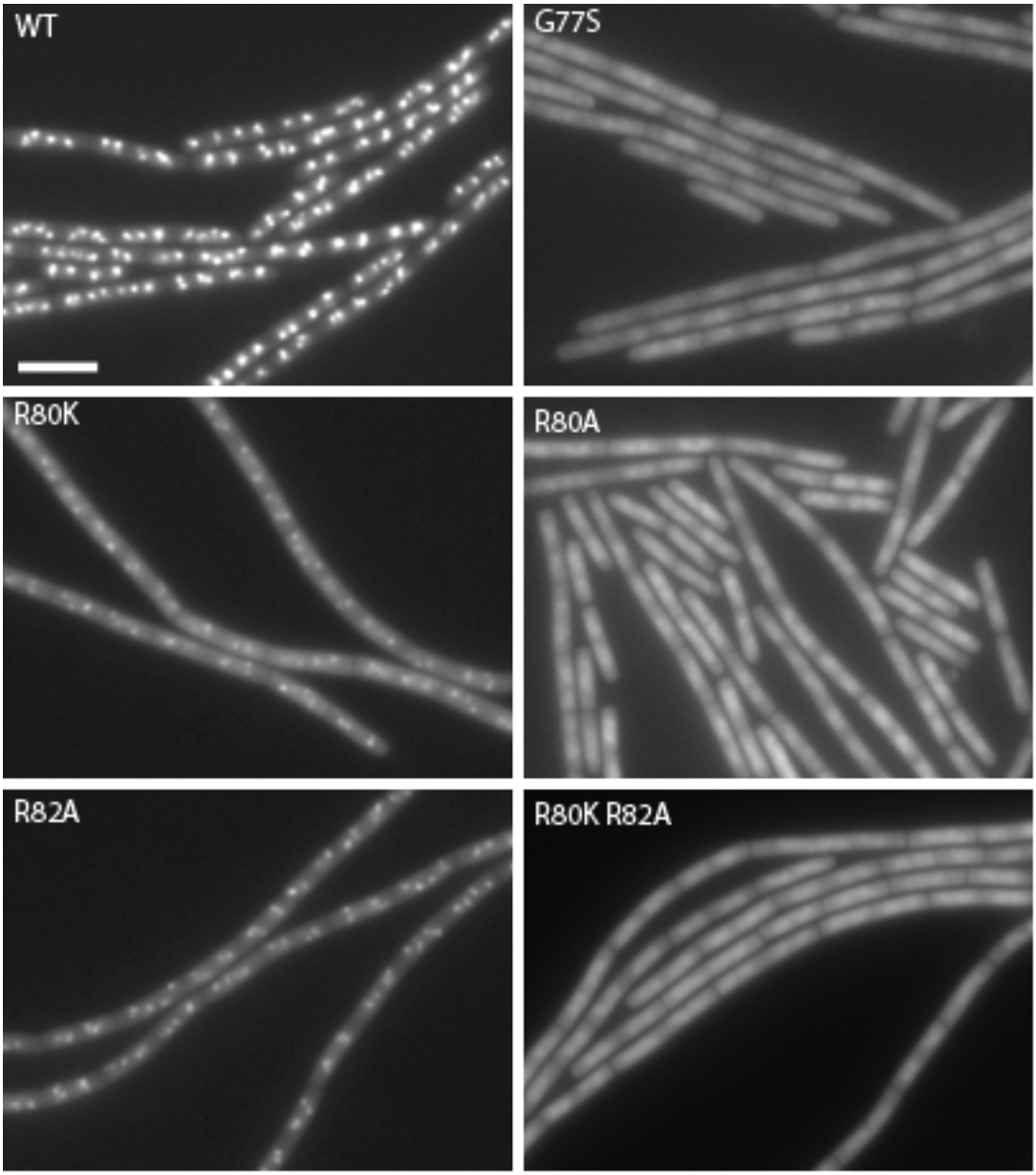

Supplemental Figure 3: Larger images of GFP-Spo0J strains shown in Figure 4c. GFP signal is shown in grayscale. Foci are still present in the R80K and R82A mutants but are much weaker than those formed by wild-type Spo0J. GFP-Spo0J^{G77S} forms even fainter and more sporadic foci. GFP-Spo0J^{R80A} and GFP-Spo0J^{R80A,R82A} form no discernable foci and show diffuse, nucleoidal localization. As in Figure 4c, all images are adjusted to have the same brightness and contrast. Scale bar = 4 µm.

Supplemental Figure 4

a

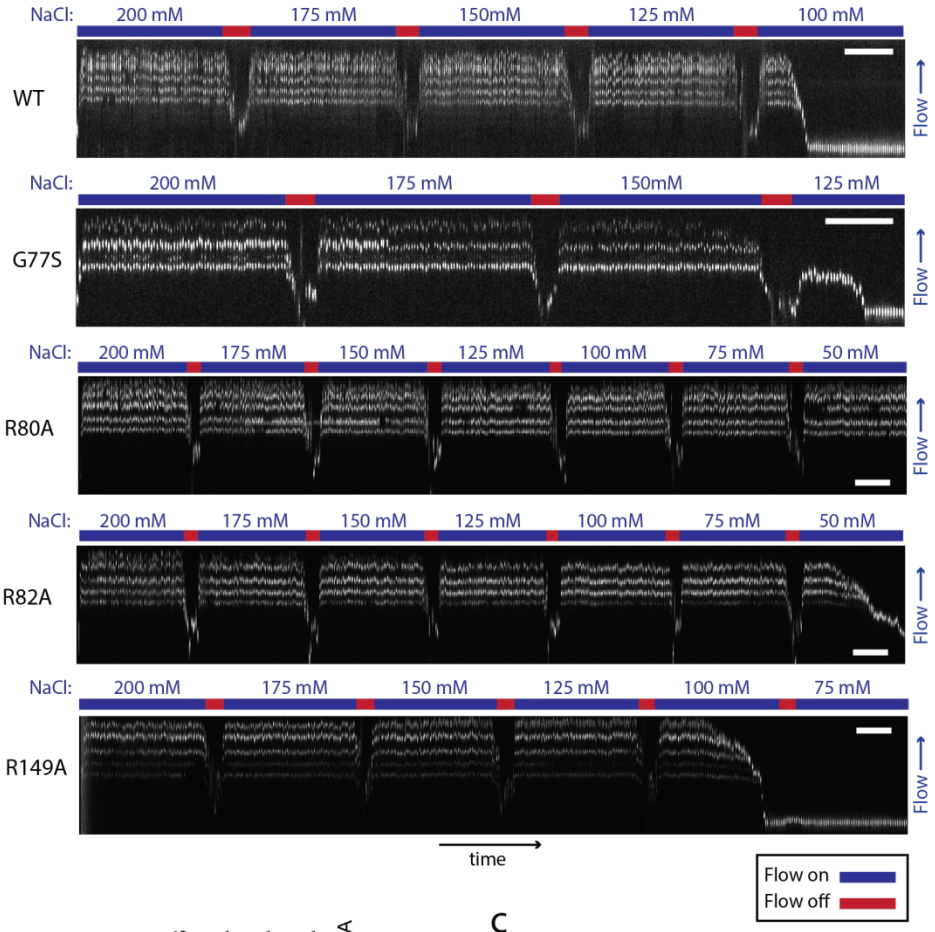

b

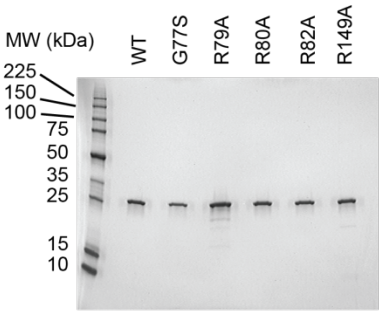

c

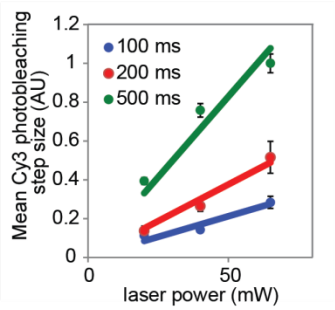

d

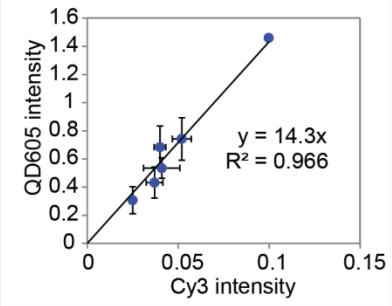

e

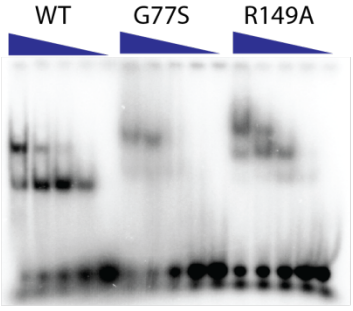

Supplemental Figure 4: (a) Salt concentration dependence of compaction by wild-type and mutant Spo0J proteins. Flow-stretched EcoRI-QD-labeled DNAs were incubated sequentially with 100 nM protein in buffers of decreasing salt concentration (blue bars), interspersed with 30 s pauses in the flow (red bars). Compaction by wild-type Spo0J occurred efficiently at a NaCl concentration of 100 mM and was suppressed by higher NaCl concentrations. Compaction by G77S began at a higher NaCl concentration of 150 mM and went to completion at 125 mM NaCl. (Note that some compaction occurred while the flow was turned off between the 150 mM and 125 mM NaCl conditions.) R80A failed to compact DNA at any NaCl concentration, while compaction by R82A occurred only at a very low NaCl concentration of 50 mM. Compaction by R149A occurred at 100 mM NaCl, albeit more slowly than compaction by wild-type Spo0J. (b) Coomassie-stained SDS-PAGE gel showing wild-type and mutant Spo0J proteins purified by H6-SUMO tandem affinity purification followed by polishing on SP sepharose. (c) Photobleaching step size of individual Cy3 fluorophores (arbitrary units) as a function of laser power for different camera exposure times, showing an approximately linear relationship between single-fluorophore intensity and laser power. Shown are means ± 2 standard errors. Lines are linear fits with y-intercept set to 0. (d) Average intensity of surface-adsorbed 605-nm quantum dots versus average intensity of individual Cy3 molecules within the same field of view. Different points represent different combinations of laser power and frame rate. Shown are means ± 2 standard errors. The slope of the best fit line, 14.3, was used to calculate the intensity per Cy3 molecule given the average quantum dot intensity in Cy3-Spo0J DNA binding experiments (see Materials and Methods). (e) Electrophoretic mobility shift assay (EMSA) of wild-type Spo0J and the G77S and R149A mutants, showing qualitatively anomalous patterns of shifted bands for these two mutants. Protein concentrations were 1, 0.75, 0.5, 0.25, and 0.1 μM.

Supplemental Figure 5:

a

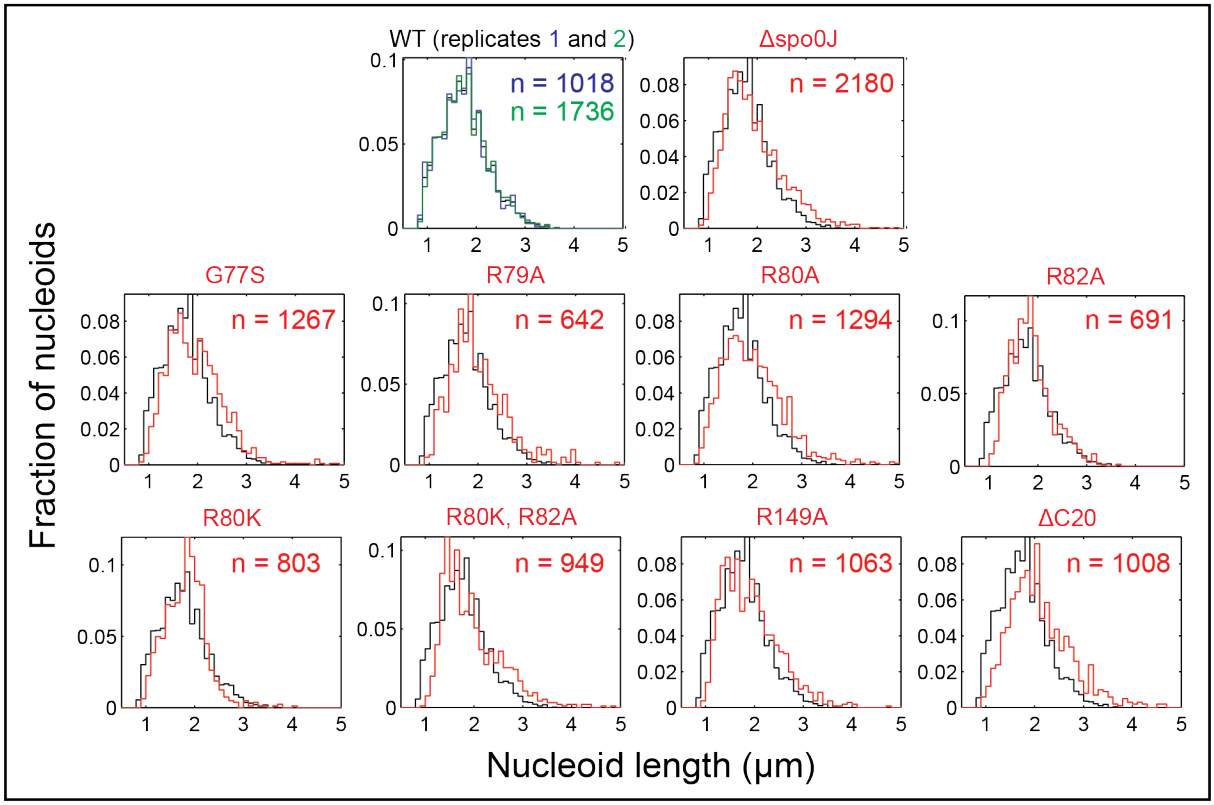

b

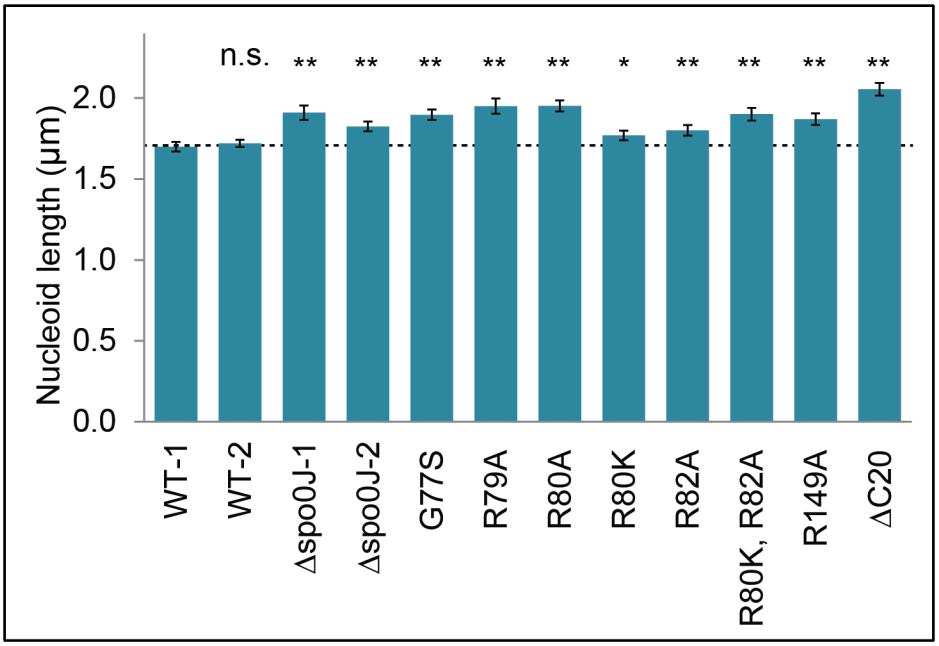

Supplemental Figure 5: Spo0J foci-defective mutants are associated with abnormal elongation of nucleoids. (a) Nucleoid length distributions of cells bearing wild-type Spo0J or different Spo0J mutants. The histogram of nucleoid lengths in wild-type cells (combined data from two replicates) is repeated for comparison in every panel (black outline). Blue and green outlines in the first panel show data from two biological replicates with wild-type cells. Red outlines in the remaining panels are nucleoid length histograms for different mutants. Numbers of cells analyzed for each condition (n) are shown. Data from two Δ*spo0J* replicates, shown separately in (b), are pooled here for clarity. (b) Average nucleoid length in wild-type and Spo0J mutant cells. Nucleoids were significantly elongated in all Spo0J mutants compared to wild-type (* $p < 0.05$; ** $p < 0.0001$, based on a Bonferroni-corrected 2-tailed t-test allowing unequal variances). Nucleoids in Spo0J loss-of-function mutants show a subtle yet reproducible increase in average length.

Supplemental Movie Legends

Supplemental Movie 1: Compaction of EcoRI-QD-labeled λ DNA by Spo0J-WT, corresponding to Figure 2c. Data are presented at 2x normal speed and are smoothed for clarity. A stationary quantum dot is nonspecifically bound to the surface in the lower right corner.

Supplemental Movie 2: Compaction of EcoRI-QD-labeled λ DNA by HBsu, corresponding to Figure 2d. Data are presented at 2x normal speed and are smoothed for clarity.

Supplemental Movie 3: Comparison of Cy3-labeled Spo0J-WT and Spo0J-R80A interactions with single DNA molecules. Cy3-labeled Spo0J-WT (left panel) compacts DNA and crosslinks adjacent DNAs, whereas Spo0J-R80A does not compact DNA and fails to crosslink adjacent DNAs (right panel). Data are presented at 8x normal speed and are smoothed for clarity. For visualization purposes, the movies on the left and the right were scaled proportional to the average intensity of DNA-bound quantum dots measured in the same channel at the beginning of the experiment (see Materials and Methods), and background fluorescence due to protein in solution was subtracted frame-by-frame. A few quantum dot-labeled DNAs are visible in the right panel.

Supplemental Table 1: Chain size and origin number for calculation of cellular Spo0J concentration

Expt.	Cells per chain				Total chains	Total cells	Average cells per chain	Total number of origins	Origins per cell
	1	2	3	4					
1	40.7%	56.4%	0.6%	2.3%	521	857	1.64	2674	3.12
2	42.5%	54.0%	0.7%	2.8%	570	934	1.64	2903	3.11
3	41.0%	56.1%	0.9%	2.0%	451	739	1.64	2310	3.13

Cells with an origin-proximal *tetO48* array that expressed the cell separase LytF, cytoplasmic mCherry, and TetR-CFP (Figure 1b) were grown under the same conditions as the cells used in the quantative immunoblot (Figure 1a). The mCherry signal was used to define the outline of the cells, and the number of CFP foci per cell was determined using MicrobeTracker (Sliusarenko et al, 2011). The number of individual cells per chain was quantified manually. Three independent experiments were analyzed. See Materials and Methods for details.

Supplemental Table 2: Summary of Spo0J mutant phenotypes

	In vivo phenotypes		In vitro properties		
	Focus formation	**Spreading**	**DNA compaction**	***parS* binding**	**References**
WT	+	+	+	+	-
G77S	-[a]	-[b]	++	+/-[c]	(Ireton et al. 1994a; Breier and Grossman 2007)
R79A	-	-	-	+	This work
R80A	-	-	-	+	(Autret et al. 2001)
R82A	+/-	ND	+/-[d]	+	This work
R80K	+/-	ND	+	ND	This work
R80K, R82A	-	ND	ND	ND	This work
R149A	-	ND	+/-	+/-[c]	(Autret et al. 2001)
ΔC20	-	ND	-	-	(Murray et al. 2006)
ΔC60	-	ND	-	-	Analogous to C-terminal truncation mutant of *T. thermophilus* Spo0J used for structure determination (Leonard et al. 2004)

Highlighted mutants are those in the ParB Box II.

+ = normal/wild type; +/- = partially deficient or anomalous; - = highly deficient; ++ = greater than wild-type; ND = not determined

[a] Extremely faint foci were observed for G77S.

[b] This work and (Breier and Grossman 2007)

[c] Anomalous electrophoretic mobility observed in EMSA experiments.

[d] Compaction only observed at very low salt (50 mM NaCl).

Supplemental Materials and Methods

Protein expression and purification

Wild-type and mutant Spo0J proteins, ParB homologs, and HBsu were expressed with an N-terminal H6-SUMO tag in BL21 cells and purified by a two-step tandem affinity method. Cell pellets were lysed by sonication in lysis buffer (20 mM Tris, pH 8, 1 M NaCl, 10 mM imidazole, 5 mM BME), and supernatants were clarified by ultracentrifugation for 1 h at 25,000 rpm in an SW-41 rotor. The clarified supernatant was bound to NiNTA resin (Qiagen) for 1 h, washed sequentially with lysis buffer and salt-reduction buffer (lysis buffer with only 350 mM NaCl) and manually eluted with a 10-100% gradient of elution buffer (20 mM Tris, pH 8, 350 mM NaCl, 300 mM imidazole, 5 mM BME) in 10% increments. Peak fractions were collected and treated with H6-tagged Ulp1 protease while dialyzing overnight at 4°C against dialysis/storage buffer (20 mM Tris, pH 8, 350 mM NaCl, 10% glycerol, 10 mM imidazole, 5 mM BME). The dialyzed protein was spun at maximum speed for 10 min in a microcentrifuge to remove precipitate (which was minimal), and the supernatant was incubated again with NiNTA resin for 1.5 h. The flowthrough, containing untagged Spo0J, was collected. For DNA compaction experiments with Spo0J, additional purification was performed by diluting the Ulp1-cleaved Spo0J protein 10-fold in SP binding buffer (50 mM MES, pH 6.5, 10% glycerol, 5 mM BME), binding to SP-sepharose, washing with SP wash buffer (50 mM MES, pH 6.5, 10% glycerol, 300 mM NaCl, 5 mM BME) and eluting in SP elution buffer (50 mM MES, pH 6.5, 10% glycerol, 450 mM NaCl, 5 mM BME), whose ionic strength had previously been optimized by gradient elution experiments. Three-step SP-purified protein was highly pure and behaved similarly to 2-step H6-SUMO-purified protein (Supplemental Figure 4b and data not shown). C-terminally KCK-tagged wild-type Spo0J (used in Figures 2-3 and Supplemental Figure 2) and N-terminally KCK-tagged wild-type Spo0J and Spo0J-R80A (used in Figure 5) were expressed and purified similarly. KCK-tagged Spo0J protein was labeled in 20 mM Tris, pH 7.5, 350 mM NaCl, 10% glycerol with a >10-fold molar excess of Cy3-maleimide dye following the manufacturer's instructions (GE Healthcare Life Sciences). Labeled protein was separated from free dye using Zeba spin desalting columns (Thermo Scientific).

H-NS-H6 purification: BL21 (DE3) cells transformed with pLS015 were grown in 500 ml LB + 50 µg/ml kanamycin at 37°C to an OD600 of 0.6. Protein expression was induced by adding IPTG to 0.8 mM, and cells were grown at 30°C for 3 h. Cell pellets were resuspended in 10 ml lysis buffer (20 mM Tris, pH 8, 1 M NaCl, 10 mM imidazole, 5 mM BME) with 500 µg/ml lysozyme and incubated at 4°C for 30 min. Cells were lysed by sonication, and the lysate was ultracentrifuged at 25,000 rpm in a SW-41 rotor for 1 h at

4°C. The clarified supernatant was incubated with 1 ml NiNTA agarose (Qiagen) for 1 h at 4°C, after which the resin was washed with 50 ml lysis buffer and 10 ml salt reduction buffer (20 mM Tris, pH 8, 350 mM NaCl, 10 mM imidazole, 5 mM BME). H-NS-H6 protein was then eluted with a 10-100% linear gradient of elution buffer (20 mM Tris, pH 8, 350 mM NaCl, 250 mM imidazole, 5 mM BME). Peak fractions were collected and dialyzed two times against 1 L 20 mM Tris, pH 8, 350 mM NaCl, 10% glycerol, 10 mM imidazole, 5 mM BME.

H6-EcoRI^{E111Q} was purified by adapting a previously published protocol (Finkelstein et al. 2010). BL21 cell pellets were lysed by sonication in buffer R (50 mM Tris-HCl, pH 7.5, 300 mM NaCl, 10% sucrose, 0.1 mM PMSF, 5 mM BME, 10 mM imidazole, complete protease inhibitor cocktail [Roche]), and the clarified supernatant was bound to NiNTA resin, washed sequentially with buffer R + 1 M NaCl and buffer R + 1 M NaCl + 50 mM imidazole, and eluted with buffer R + 250 mM imidazole without protease inhibitors. Eluates were dialyzed against buffer S (60 mM Tris-HCl, pH 7.5, 450 mM NaCl, 15 mM BME, 0.15 mM EDTA, 10% glycerol, 0.21% Triton X-100), and 1 part glycerol was added to 2 parts dialysate for storage.

Single-molecule imaging

Single-molecule experiments were carried out in flow cells assembled as previously described (Tanner et al. 2008). A functionalized coverslip passivated with a mix of high molecular weight polyethylene glycol (PEG) and PEG-biotin served as the bottom surface of the flow cell. Addition of streptavidin to the flow cell allowed for the tethering of biotinylated DNA substrates. DNAs were extended under flow by pulling buffer through the flow cell with a syringe pump (Harvard Apparatus). Quantum dots and Cy3-labeled Spo0J were imaged with a homebuilt through-objective TIRF microscope using 532 nm excitation (Coherent, Compass 215M-75). The expanded and collimated laser beam was focused through the rear port of an inverted microscope (Olympus, IX71) and onto the back aperture of a high-NA objective (Olympus, NA 1.45). The beam was vertically translated across the objective by a focusing lens to give total internal reflection. The filtered fluorescence emission (Chroma) was imaged onto an electron multiplying charge-coupled device camera (Hamamatsu, EM-CCD 9100-13). For experiments that simultaneously imaged both Cy3-labeled Spo0J and 705 nm quantum dots, the fluorescence signals were spectrally separated in a homebuilt dual-view apparatus, filtered, and imaged onto separate halves of the EM-CCD.

Generation of lambda-parS *DNA*

A kanamycin resistance cassette was amplified from pKD13 (Datsenko and Wanner 2000) using primers odr790 and odr792. These primers contain respectively 40 and 50 bp of homology to an internal site in lambda DNA. The forward primer additionally contains a *parS* site. The PCR product was electroporated into a lysogen, *E. coli* MC4100 (*λ cI857 Sam7*) (Wang 2006) to replace two non-essential genes (*stf* and *tfa*) in the prophage using a recombineering method described previously (Thomason et al. 2009). The resulting construct (λ^{parS}) was confirmed by sequencing using primers odr793, odr794, and odr795. To purify lambda DNA, a 500 ml culture of the λ^{parS} lysogen strain was grown exponentially at 30˚C and shifted to 42°C for 2 h to induce lysis. 1 ml chloroform was added to the shaking lysate for 2 min. After treating with DNase I (500 U) and RNase I (500 μg) at room temperature for 30 min, solid NaCl was added to a final concentration of 1 M, and the lysate was clarified by centrifugation at 11,000 *g* for 10 min at 4°C. To precipitate phage particles, 50 g of PEG 8000 were added with slow stirring, and the mixture was incubated in an ice water slurry for 1 h. Phages were pelleted by centrifugation at 11,000 *g* for 10 min at 4°C, resuspended in 8 ml lambda dilution buffer (10 mM Tris, pH 7.4, 5 mM $MgSO_4$, 0.01% gelatin), and extracted once with chloroform. The aqueous phase was ultracentrifuged at 83000 *g* for 2 h at 4°C to recover phage particles. The pellet was resuspended thoroughly in 2 ml lambda dilution buffer and incubated with 0.5% SDS and 50 μg/ml proteinase K for 1 h at 56°C. The solution was gently extracted with equal volumes phenol, 25:24:1 phenol:chloroform:isoamyl alcohol, and 24:1 chloroform:isoamyl alcohol, and the aqueous phase was dialyzed three times against 1 liter 1x TE.

Measurement of Cy3-Spo0J binding density on lambda DNA

In order to determine how many molecules of Cy3-labeled Spo0J bound per length of DNA, we used the average intensity of 605-nm quantum dots as an “standard candle” to compare intensities between single-fluorophore and many-fluorophore imaging conditions. We first determined the average intensities of 605-nm quantum dots and individual Cy3 fluorophores adsorbed on a surface at several different laser powers and exposure times (Supplemental Figure 4c-d). The ratio between average QD605 fluorescence and average Cy3 fluorescence remained similar under different conditions (Supplemental Figure 4d), and we used the slope of the best-fit line (14.3) as a conversion factor between average QD605 intensity and average Cy3 intensity. In other words, we estimate that under the same imaging conditions, the average QD605 gives a signal 14.3 times that of the average Cy3 molecule.

We determined the labeled fraction of Cy3-Spo0J^{WT} and Cy3-Spo0J^{R80A} proteins by running a dilution series of the labeled protein on an SDS-PAGE gel alongside dilution series of a protein standard (bovine serum albumin) and a Cy3 standard (a Cy3-labeled oligonucleotide) of known concentration. Cy3 was imaged using a Typhoon imager, the gels were immediately stained with InstantBlue Coomassie Stain (Expedeon), and Coomassie staining was imaged on a GDS-8000 imaging system (UVP BioImaging Systems). Band intensities were measured in ImageJ. Cy3 and protein concentrations in the labeled sample were determined by comparison with the standard curves, and the labeled fraction was determined as the molar ratio of Cy3 to protein.

For quantitative DNA binding and compaction experiments with labeled protein (Figure 5c), a small concentration of lambda DNA was labeled with H6-EcoRI^{E111Q} and anti-H6 605 QDs as described in the main text and tethered to a functionalized glass surface in a 2 mm-wide microfluidic channel. QD-labeled DNAs were extended by flowing 20 mM Tris, pH 7.5, 100 mM NaCl, 100 µg/ml BSA through the channel at a flow rate of 50 µl/min, and DNA-bound quantum dots were imaged with a 100 ms frame acquisition time and 2 s between frames. Unlabeled lambda DNA at a higher concentration was then tethered in the same channel. Cy3-labeled Spo0J$^{WT/R80A}$ and unlabeled Spo0J$^{WT/R80A}$ were diluted in 20 mM Tris, pH 7.5, 100 mM NaCl, 100 µg/ml BSA to give a final protein concentration of 100 nM and a final labeled fraction of 5%. This mixture was pulled into the channel at 50 µl/min while imaging under the same conditions used to image the quantum dots. Cy3-Spo0J-WT compacted DNA under these conditions, but Cy3-Spo0J^{R80A} did not. After the experiment, the average intensity of quantum dots in the initial movies was determined manually in ImageJ (average of >100 QDs per experiment). The number of dimers bound per kilobase of DNA was calculated from the background-subtracted integrated intensity of Cy3 on the DNA using the formula:

(dimers per kb) = (intensity on DNA) * 14.3 / ((average QD intensity) * 0.05 * 2 * 48.5),

where 14.3 is the ratio of QD to Cy3 intensities, 0.05 is the monomer labeling fraction, and 48.5 is the length of lambda DNA in kilobases. Only well-separated full-length lambda DNAs were included in the analysis shown in Figure 5c (n = 14 from 3 separate experiments for Cy3-Spo0J-WT and n = 6 from 2 separate experiments for Cy3-Spo0J-R80A).

Electrophoretic mobility shift assay (EMSA) experiments

Oligonucleotides oTG041F and oTG041R were annealed in 1x TE + 50 mM NaCl, labeled with ^{32}P by phosphorylation with T4 polynucleotide kinase (NEB), and purified away from

the free label using illustra MicroSpin G50 spin desalting columns (GE Healthcare Life Sciences). Protein, diluted to 10 times the indicated concentrations in storage buffer, was added to labeled *parS* oligo duplex (5 nM) plus scrambled competitor oligo duplex (50 nM; formed by annealing oTG043F and oTG043R) in binding buffer (20 mM Tris pH 7.5, 300 mM NaCl). 10 µl reactions were assembled on ice and then incubated at room temperature for 10 min. 5 µl of loading dye (20 mM Tris pH 7.5, 300 mM NaCl, 48% glycerol, and trace amounts of bromophenol blue) were added to each reaction, and 5 µl of each were loaded on a 5% 0.5x TBE-PAGE gel, which was run at 200 V for approximately 20 min. Gels were dried, exposed to a storage phosphorscreen, and imaged on a Personal Molecular Imager (BioRad).

Immunoblot analysis

Whole cell lysates from vegetatively growing cells were prepared as described (Doan and Rudner 2007). Samples were heated for 10 min at 55°C prior to loading. Equivalent loading was based on OD600 at the time of harvest. Proteins were separated by SDS-PAGE on 12.5% polyacrylamide gels, electroblotted onto Immobilon-P membranes (Millipore) and blocked in 5% nonfat milk in phosphate-buffered saline (PBS)-0.5% Tween-20. The blocked membranes were probed with anti-Spo0J (1:5,000) (Lin et al. 1997), anti-GFP (1:10,000) (Rudner et al. 1999) or anti-SigA (1:10,000) (Fujita 2000) diluted into 3% BSA in 1x PBS-0.05% Tween-20. Primary antibodies were detected using horseradish peroxidase-conjugated goat anti-rabbit IgG (BioRad) and the Super Signal chemiluminscence reagent as described by the manufacturer (Pierce).

Quantitative immunoblot

Because wild-type *Bacillus subtilis* grows in chains, the number of colony forming units (CFU) underestimates the total number of cells in the culture. To quantify the number of proteins per cell, we used a strain (BJM745) in which the cell wall separase (LytF) was expressed under IPTG control. In the presence of inducer (0.5 mM IPTG), cells predominantly grow as singlets or doublets (Fig. 1b). Through serial dilution and plating (in duplicate), it was determined that the culture had 3.6×10^8 cfu/ml/OD.
To determine the average number of founder cells per CFU (i.e. the average number of cells per chain) and the number of origins per cell, cells that express the cell separase (LytF), cytoplasmic mCherry, TetR-CFP and possess *tetO48* adjacent to the replication origin were grown under the same conditions (see below) as the cells used for the quantitative immunoblot. Using MicrobeTracker (see Analysis of Bacterial Images), it was determined that there were, on average, 3.1 origins per cell and, on average, 1.6 cells per chain (Supplemental Table 1). Three independent experiments were analyzed.

For the quantitative immunoblot, cells (BJM745) were grown in defined rich (CH) medium to an optical density of 0.5. Under these conditions, cells grew with a doubling time of 32 minutes. Whole cell lysates were prepared from 1 ml of culture (see Immunoblot analysis). A Δ*spo0J* mutant strain (BDR1873) was processed identically. The Δ*spo0J* lysate was used to dilute the wild-type cell lysate and the purified protein so that all samples contained the same amount of whole cell lysate. The equivalent of 100 µl cell lysate (A_{600} = 0.5) was loaded in each lane. The blocked membrane was probed with anti-Spo0J antibodies (Lin and Grossman 1998) diluted into 3% BSA in 1x PBS-0.05% Tween-20. Primary antibodies were detected using horseradish peroxidase-conjugated goat anti-rabbit IgG (BioRad) and the Super Signal chemiluminscence reagent as described by the manufacturer (Pierce). The signal was captured using Bio-Rad ChemiDoc XRS and the intensity of each band was quantified using Quantity One software. A standard curve was generated by plotting the intensity of the bands against different amounts of purified untagged Spo0J protein loaded. The amount of protein in the cell lysate was calculated using the standard curve. Three independent experiments were analyzed.

The concentration of purified untagged Spo0J protein was first estimated using Coomassie Plus (Bradford) Assay Kit (Thermo Scientific) according to the manufacturer's instructions. Serial dilutions of the purified protein and a bovine serum albumin (BSA) standard were run on an SDS-PAGE gel, stained with Coomassie Blue, and quantified using imaging software to more accurately estimate the protein concentration. Specifically, BSA (2 µg/µl, Thermo Scientific) was diluted to 0.2 µg/µl, 0.1 µg/µl, 0.05 µg/µl, 0.025 µg/µl and 0.0125 µg/µl using Spo0J storage buffer (20 mM Tris pH 8.0, 350 mM NaCl, 10 mM imidazole, 10% glycerol, 5 mM BME). Using the concentration estimated with the Bradford assay, the purified Spo0J protein was serially diluted to the same range of concentration as the BSA standard. 10 µl of each dilution of BSA and Spo0J were run on a 12.5% SDS-PAGE gel. The gel was stained with Coomassie Blue and imaged using a Bio-Rad ChemiDoc XRS imager. The intensity of individual bands was quantified using Image Lab 3.0 software. A BSA standard curve was generated by plotting the intensity of the band against the amount of BSA protein loaded. The intensity of the Spo0J bands was fit into the linear part of the standard curve to calculate the concentration. Two independent experiments were performed to calculate the concentration. The concentration of the protein was 0.75 ± 0.07 µg/µl. Estimates between the solution Bradford and SDS-PAGE/Coomassie methods differed by < 10%.

Analysis of bacterial images

Image analyses were performed using the MATLAB-based program, MicrobeTracker (Sliusarenko et al. 2011). Nucleoid outlines were determined using the DNA fluorescent

dye (DAPI) or fluorescent fusions to the nucleoid-associated protein HBsu (HBsu-mYpet or HBsu-mGFPmut3). Where these fluorescence signals were used for segmentation, the background fluorescence intensity was determined by averaging the fluorescence intensity in cell-free regions of the image and subtracted from the image in MetaMorph. After background subtraction, the images were then inverted in MicrobeTracker and analyzed using built-in algorithms in MicrobeTracker. After segmentation, MicrobeTracker generated a coordinate system for each cell (or nucleoid where DAPI or HBsu fusions were used), called a mesh, in which each point was described by two coordinates: the distance to a cell pole that was randomly selected and the distance to the mid-line along the cell length. The mesh was used to calculate cell (or nucleoid) length, width, and area. In Figure 1b and Supplemental Table 1, the outlines of individual cells were determined in MicrobeTracker using cytoplasmic mCherry expressed under the control of a constitutive promoter, Pveg (Fukushima et al. 2003). Subsequently, the number of individual cells in each chain (or CFU) was quantified manually. The number of origin foci per cell was determined using SpotFinder in MicrobeTracker.

ChIP-seq

Chromatin immunoprecipitation (ChIP) was performed as previously described (Wagner-Herman et al. 2012). Cells were grown in defined rich (CH) medium to an optical density of 0.5. Formaldehyde was added to 20 ml of cells to a final concentration of 1%, and samples were incubated for 10 min at room temperature. Crosslinking was quenched by the addition of glycine to a final concentration of 125 mM and incubation at room temperature for 5 min. Cell pellets were then washed twice with 1x PBS and treated with lysozyme (1 mg/ml final) for 15 min in buffer A (12.5 mM Tris pH 8, 12.5 mM EDTA, 62.5mM NaCl, 25% sucrose, 1 mM PMSF), followed by the addition of Triton X-100 to a final concentration of 1%. Chromosomal DNA was sheared to an average size of 300 bp by sonication using a Misonix Ultrasonic Liquid S-4000. After the removal of cell debris by centrifugation, 50 µl was removed to serve as an input control. The lysate was incubated overnight at 4˚C with affinity-purified anti-Spo0J antibodies and was then incubated with Protein A-sepharose resin (GE HealthCare) for 1 h at 4˚C. The resin was washed 3 times with IP Buffer (50 mM Tris pH 7.5, 5 mM EDTA, 150 mM NaCl, 1% Triton), 3 times with Wash Buffer (50 mM Tris pH 7.5, 1 mM EDTA, 500 mM NaCl, 1% Triton), and once with 1x TE (50 mM Tris pH 8, 10 mM EDTA). The resin was then resuspended in elution buffer (50 mM Tris pH 8, 10 mM EDTA pH 8, 1% SDS) and incubated at 65˚C for 15 min. The recovered supernatants and the input control samples were placed at 65˚C overnight to reverse the crosslinks. The samples (input and IP) were treated with RNase A (200 µg/ml final concentration) at 37°C for 1 h, followed by incubation with proteinase K (0.2 mg/ml final concentration). The DNA was purified by phenol-chloroform extraction and ethanol precipitation, followed by

purification with AmpureXP beads (Beckman Coulter, Inc.). 2-5 ng of chromatin immunoprecipitated DNA and control DNA was prepared for Illumina HiSeq high-throughput sequencing using the NEBNext ChIP-Seq library prep reagent set for Illumina (NEB #6200). The sequencing reads were aligned to the *B. subtilis* 168 genome (NC000964) using CLC Genomics Workbench software. CLC Genomics Workbench ChIP coupled with next-generation sequencing (ChIP-seq) software was used to compare ChIP samples and input control to calculate enrichment. Two biological replicates were sequenced for each sample. Enrichment was normalized to the total number of reads for each sample.

Strain construction

∆spo0J (∆parS)::spec was obtained by direct transformation of an isothermal assembly product (Gibson et al. 2009) into the wild-type strain PY79. The isothermal assembly reaction contained three PCR fragments: 1) a 0.7 kb region upstream the *spo0J* gene (amplified from wild-type genomic DNA using primers oWX507 and oWX886); 2) a *loxP-spec-loxP* cassette (amplified from pWX466 using primers oWX438 and oWX439), and 3) a 1.6 kb region downstream of the *spo0J* gene (amplified from wild-type genomic DNA using primers oWX887 and oWX888). pWX466 contains a *loxP-spec-loxP* cassette (X.W. and D.Z.R., unpublished). The resulting construct was sequenced across the *soj-spo0J* region using primers oWX507 and oWX508. This construct deletes the *parS* site that is present within the *spo0J* gene, whereas *∆spo0J::spec* in AG1468 (Ireton et al. 1994b) retains the *parS* site at this locus.

Plasmid construction

pTG004 was generated by cloning EcoRI^{E111Q} (PCR amplified from the E111Q derivative of pSCC3 (Wright et al. 1989) with oTG001F and oTG001R) into pET28b cut with NheI and EcoRI to generate an N-terminally H6-tagged fusion.

pKM397 was generated by cloning *hbs* (PCR amplified from PY79 genomic DNA using odr802 and odr803 and digested with SapI and XhoI) into pTB146 [H6-SUMO expression plasmid] (T. Bernhardt, unpublished) between SapI and XhoI.

pKM304 was generated by cloning *spo0J* (PCR amplified from PY79 genomic DNA using odr665 and odr666 and digested with SapI and XhoI) into pTB146 [H6-SUMO expression plasmid] (T. Bernhardt, unpublished) between SapI and XhoI.

Variants of **pKM304** were generated by site-directed mutagenesis with the following primer pairs:

pTG052	oTG049F and oTG049R
pTG118	oTG167 and oTG168
pTG037	oTG027F and oTG027R
pTG169	oTG212 and oTG224
pTG119	oTG169 and oTG170
pTG105	oTG143 and oTG144
pTG107	oTG026F and oTG026R
pTG050	oTG037F and oTG037R
pTG036	oTG025F and oTG025R

pTG029 was generated from **pKM304** by site-directed mutagenesis with primers oTG024F and oTG024R.

pTG042 was generated from **pKM304** by site-directed mutagenesis with primers oTG039F and oTG039R.

pTG044 was generated from **pTG042** by site-directed mutagenesis with primers oTG027F and oTG027R.

pTG051 was generated from **oTG029** by site-directed mutagenesis with primers oTG038F and oTG038R.

pTG043 was generated from **pTG036** by site-directed mutagenesis with primers oTG039F and oTG039R.

pTG098: A PCR product encoding *parB* was PCR amplified from *Pseudomonas aeruginosa* PAO1 genomic DNA using primers oTG133 and oTG134, cut with BamHI and SalI, and ligated into pH6-SUMO cut with BamHI and XhoI.

pTG099: A PCR product encoding *parB* was PCR amplified from a *Streptococcus pneumoniae* genomic DNA using primers oTG135 and oTG136, cut with BamHI and XhoI, and ligated into pH6-SUMO cut with the same enzymes.

pTG101: A PCR product encoding *parB* was PCR amplified from a P1 phage lysate using primers oTG122 and oTG123, cut with BamHI and XhoI, and ligated into pH6-SUMO cut with the same enzymes.

pWX563 was generated in a 3-way ligation to insert *mgfpmut3* (amplified from pDHL580 (Landgraf et al. 2012)) using primers oWX706 and oWX674 and digested with HindIII and XhoI) and *spo0J (ΔparS)* (excised from pKM256 using XhoI and BamHI) into pWX516 between HindIII and BamHI. pKM256 contains *pelB::Psoj-gfp-spo0J(ΔparS) (cat)*, where *spo0J (ΔparS)* has 7 synonymous changes in the 16-base *parS* site in the *spo0J* gene (Sullivan et al. 2009). pWX516 contains *pelB::Psoj (tet)* (X.W. and D.Z.R., unpublished).

Variants of **pWX563** were generated by site-directed mutagenesis with the following primer pairs:

pTG138	oTG049F and oTG049R
pTG140	oTG167 and oTG168
pTG141	oTG027F and oTG027R
pTG158	oTG212 and oTG224
pTG197	oTG284 and oTG285
pTG142	oTG169 and oTG170
pTG206	oTG026F and oTG026R
pTG185	oTG249 and oTG250
pTG186	oTG247 and oTG248

pNS069: (*soj spo0J(ΔparS)*) was amplified from genomic DNA derived from DCL468 (Lin and Grossman 1998) using primers oNS24 and oNS25. The product was cut with BamHI and EcoRI and inserted into pKM20 between EcoRI and BamHI. pKM20 (K. Marquis and D.Z.R, unpublished) contains *pelB::cat*.

Variants of **pNS069** were generated by site-directed mutagenesis with the following primer pairs:

pTG123	oTG049F and oTG049R
pTG182	oTG167 and oTG168
pTG122	oTG027F and oTG027R
pTG147	oTG212 and oTG224
pTG134	oTG143 and oTG144
pTG183	oTG026F and oTG026R
pTG198	oTG251 and oTG252

pWX610 was generated by inserting *PftsW-tetR-cfp* (excised from pWX193 using EcoRI and BamHI) into pWX137 between EcoRI and BamHI sites, replacing *Ppen-tetR-mCherry.* pWX193 (X.W. and D.Z.R. unpublished) has *ycgO::PftsW-tetR-cfp (spec).* pWX137 (X.W. and D.Z.R. unpublished) has *yhdG::Ppen-tetR-mCherry (spec).*

pWX611 was generated in a 3-way ligation to insert *mgfpmut3* (PCR amplified from pDHL580 (Landgraf et al. 2012)) using primers oWX706 and oWX674 and digested with HindIII and XhoI) and *spo0J (ΔparS)-KCK* (PCR amplified from the genomic DNA of DCL468 (Lin and Grossman 1998) using oWX1086 and oWX1087, and digested with XhoI and BamHI) into pKM170 between HindIII and BamHI. pKM170 (K. Marquis and D.Z.R., unpublished) contains *pelB::Psoj (cat).*

pWX612 was generated by inserting *soj-spo0J (ΔparS)-KCK* (PCR amplified from the genomic DNA of DCL468 (Lin and Grossman 1998) using primers oNS24 and oWX1087

and digested with EcoRI and BamHI) into pKM20 between EcoRI and BamHI sites. The 5-amino-acid tag that contains a cysteine, SGKCK, was introduced by primer oWX1087. pKM20 (K. Marquis and D.Z.R, unpublished) contains *pelB::cat*.

pLS015 was generated by amplifying the *hns* gene from *E. coli* MG1655 genomic DNA using primers oLS015F and oLS015R. The PCR product was digested with NdeI and XhoI and cloned into the same restriction sites of pET24b, and the sequence of the resulting construct was confirmed by sequencing.

Strains used in this study

strain	Genotype	source	figure
BJM745	*ycgO::Pspank-lytF erm*	J. Meinsner and D.Z.R, unpublished	1a
BDR1873	*Δ(soj spo0J)::spec*	This work	1a
BDR2971	*ycgO::Pspank-lytF erm, yycR::tetO48 cat, yhdG::PftsW-tetR-CFP spec, sacA::Pveg-mCherry phleo*	This work	1b, Sup. Table 1
BDR2972	*Δspo0J::spec, pelB::Psoj-mgfpmut3-spo0J (ΔparS) tet, yycR::tetO48 cat, ycgO::PftsW-tetR-mCherry phleo*	This work	1c
BDR2973	*parSΔ4, Δspo0J (ΔparS)::spec, pelB::Psoj-mgfpmut3-spo0J (ΔparS) tet, yycR::tetO48 cat, ycgO::PftsW-tetR-mCherry phleo*	This work	1c
BDR2974	*parSΔ6, Δspo0J (ΔparS)::spec, pelB::Psoj-mgfpmut3-spo0J (ΔparS) tet, yycR::tetO48 cat, ycgO::PftsW-tetR-mCherry phleo*	This work	1c
BDR2976	*parSΔ8, Δspo0J (ΔparS)::spec, pelB::Psoj-mgfpmut3-spo0J (ΔparS) tet, yycR::tetO48 cat, ycgO::PftsW-tetR-mCherry phleo*	This work	1c
BDR2711	*pelB::Psoj-mgfpmut3-spo0J **WT** (ΔparS) tet, Δspo0J::spec*	This work	4b
BDR2710	*pelB::Psoj-mgfpmut3-spo0J **R79A** (ΔparS) tet, Δspo0J::spec*	This work	4b
BDR2713	*pelB::Psoj-mgfpmut3-spo0J **R80A** (ΔparS) tet, Δspo0J::spec*	This work	4b
BDR2849	*pelB::Psoj-mgfpmut3-spo0J **R82A** (ΔparS) tet, Δspo0J::spec*	This work	4b
BDR2716	*pelB::Psoj-mgfpmut3-spo0J **R80K** (ΔparS) tet, Δspo0J::spec*	This work	4b
BDR2851	*pelB::Psoj-mgfpmut3-spo0J **R80K R82A** (ΔparS) tet, Δspo0J::spec*	This work	4b
BDR2709	*pelB::Psoj-mgfpmut3-spo0J **G77S** (ΔparS) tet, Δspo0J::spec*	This work	4b

BDR2862	*pelB::Psoj-mgfpmut3-spo0J **R149A** (ΔparS) tet, Δspo0J::spec*	This work	4b
BDR2792	*pelB::Psoj-mgfpmut3-spo0J Δ**C20**, (ΔparS) tet, Δspo0J::spec*	This work	Sup. Table 2
BDR2793	*pelB::Psoj-mgfpmut3-spo0J Δ**C60**, (ΔparS) tet, Δspo0J::spec*	This work	4b
BDR2798	*pelB::Psoj-mgfpmut3-spo0J **WT** (ΔparS) tet, Δspo0J::spec, sacA::hbs-mcherry kan*	This work	4c
BDR2797	*pelB::Psoj-mgfpmut3-spo0J **R79A** (ΔparS) tet, Δspo0J::spec, sacA::hbs-mcherry kan*	This work	4c
BDR2799	*pelB::Psoj-mgfpmut3-spo0J **R80A** (ΔparS) tet, Δspo0J::spec, sacA::hbs-mcherry kan*	This work	4c
BDR2866	*pelB::Psoj-mgfpmut3-spo0J **R82A** (ΔparS) tet, Δspo0J::spec, sacA::hbs-mcherry kan*	This work	4c
BDR2865	*pelB::Psoj-mgfpmut3-spo0J **R80K** (ΔparS) tet, Δspo0::spec, sacA::hbs-mcherry kan*	This work	4c
BDR2868	*pelB::Psoj-mgfpmut3-spo0J **R80K R82A** (ΔparS) tet, Δspo0J::spec, sacA::hbs-mcherry kan*	This work	4c
BDR2796	*pelB::Psoj-mgfpmut3-spo0J **G77S** (ΔparS) tet, Δspo0J::spec, sacA::hbs-mcherry kan*	This work	4c
BDR2872	*pelB::Psoj-mgfpmut3-spo0J **R149A** (ΔparS) tet, Δspo0J::spec, , sacA::hbs-mcherry kan*	This work	4c
BDR2802	*pelB::Psoj-mgfpmut3-spo0J Δ**C60**, (ΔparS) tet, Δspo0J::spec, sacA::hbs-mcherry kan*	This work	4c
BDR2806	*pelB::(soj spo0J **WT** (ΔparS)) cat, Δ(soj spo0J)::spec, scpB-mgfpmut3 erm*	This work	6a-b
BDR2807	*Δspo0J::spec, scpB-mgfpmut3 erm*	This work	6a-b
BDR2805	*pelB::(soj spo0J **G77S** (ΔparS)) cat, Δ(soj spo0J)::spec, scpB-mgfpmut3 erm*	This work	6a-b
BDR2808	*pelB::(soj spo0J **R79A** (ΔparS)) cat, Δ(soj spo0J)::spec, scpB-mgfpmut3 erm*	This work	6a-b
BDR2804	*pelB::(soj spo0J **R80A** (ΔparS)) cat, Δ(soj spo0J)::spec, scpB-mgfpmut3 erm*	This work	6a-b
BDR2803	*pelB::(soj Spo0J **R149A** (ΔparS)) cat, Δ(soj spo0J)::spec, scpB-mgfpmut3 erm*	This work	6a-b
BDR2977	*pelB::Psoj-mgfpmut3-spo0J **KCK** (ΔparS) cat, Δspo0J::spec*	This work	Sup. Fig. 2g

BDR2978	*pelB::(soj spo0J **KCK** (ΔparS)) cat, Δ(soj spo0J)::spec, scpB-mgfpmut3 erm*	This work	Sup. Fig. 2h
PY79	wild type	Youngman et al., 1986	-
AG1468	*Δspo0J::spec, trpC2, pheA1*	Ireton et al., 1994	-
AG1505	*Δ(soj spo0J)::spec, trpC2, pheA1*	Ireton et al., 1994	-
BDR2637	*sacA::Pveg-mCherry phleo*	D.Z.R unpublished	-
BNS1143	*parSΔ4: spo0J (parSΔ), yycG (parSΔ) , rocR (parSΔ), cotF (parSΔ)*	N. Sullivan and D.Z.R unpublished	-
BNS1534	*parSΔ6: spo0J (parSΔ), yycG (parSΔ) , rocR (parSΔ), cotF (parSΔ), metS (parSΔ), ybbC(parSΔ)*	N. Sullivan and D.Z.R unpublished	-
BNS1657	*parSΔ8: spo0J (parSΔ), yycG (parSΔ) , rocR (parSΔ), cotF (parSΔ), metS (parSΔ), ybbC(parSΔ), ydaD(parSΔ), nfrA(parSΔ)*	Sullivan et al., 2009	-
DCL468	*spo0J (ΔparS), trpC2, pheA1*	Lin and Grossman 1998	-

Plasmids used in this study

Plasmid	Description	Source
pTG004	H6-EcoRI-E111Q/pET28b	This work
pKM397	H6-SUMO-HBsu	This work
pKM304	H6-SUMO-Spo0J	This work
pTG052	H6-SUMO-Spo0J-G77S	This work
pTG118	H6-SUMO-Spo0J-R79A	This work
pTG037	H6-SUMO-Spo0J-R80A	This work
pTG169	H6-SUMO-Spo0J-R80A	This work
pTG119	H6-SUMO-Spo0J-R82A	This work
pTG107	H6-SUMO-Spo0J-R149A	This work
pTG050	H6-SUMO-Spo0J-ΔC20	This work
pTG036	H6-SUMO-Spo0J-ΔC60	This work
pTG029	H6-SUMO-Spo0J-KCK	This work
pTG042	H6-SUMO-KCK-Spo0J	This work
pTG044	H6-SUMO-KCK-Spo0J-R80A	This work
pTG051	H6-SUMO-Spo0J-ΔC20-KCK	This work
pTG043	H6-SUMO-KCK-Spo0J-ΔC60	This work
pTG098	H6-SUMO-*P. aeruginosa* ParB	This work
pTG101	H6-SUMO-P1 ParB	This work
pTG099	H6-SUMO-*S. pneumoniae* ParB	This work
pWX563	*pelB::Psoj-mgfpmut3-spo0J (ΔparS) tet*	This work
pTG138	*pelB::Psoj-mgfpmut3-spo0J-G77S (ΔparS) tet*	This work
pTG140	*pelB::Psoj-mgfpmut3-spo0J-R79A (ΔparS) tet*	This work
pTG141	*pelB::Psoj-mgfpmut3-spo0J-R80A (ΔparS) tet*	This work
pTG158	*pelB::Psoj-mgfpmut3-spo0J-R80K (ΔparS) tet*	This work

pTG197	*pelB::Psoj-mgfpmut3-spo0J-R80K, R82A (ΔparS) tet*	This work
pTG142	*pelB::Psoj-mgfpmut3-spo0J-R82A (ΔparS) tet*	This work
pTG206	*pelB::Psoj-mgfpmut3-spo0J-R149A (ΔparS) tet*	This work
pTG185	*pelB::Psoj-mgfpmut3-spo0J-ΔC20 (ΔparS) tet*	This work
pTG186	*pelB::Psoj-mgfpmut3-spo0J-ΔC60 (ΔparS) tet*	This work
pNS069	*pelB::Psoj-soj-spo0J (ΔparS) cat*	This work
pTG123	*pelB::Psoj-soj-spo0J-G77S (ΔparS) cat*	This work
pTG182	*pelB::Psoj-soj-spo0J-R79A (ΔparS) cat*	This work
pTG122	*pelB::Psoj-soj-spo0J-R80A (ΔparS) cat*	This work
pTG147	*pelB::Psoj-soj-spo0J-R82A (ΔparS) cat*	This work
pTG183	*pelB::Psoj-soj-spo0J-R149A (ΔparS) cat*	This work
pTG198	*pelB::Psoj-soj-spo0J-ΔC20 (ΔparS) cat*	This work
pWX178	*yycR::tetO48 cat*	Wang et al 2014
pWX510	*ycgO::PftsW-tetR-mCherry phleo*	Wang et al 2014
pWX610	*yhdG::PftsW-tetR-cfp spec*	This work
pWX611	*pelB::Psoj-mgfpmut3-spo0J(ΔparS)-KCK cat*	This work
pWX612	*pelB::soj-spo0J (ΔparS)-KCK cat*	This work
pLS015	H-NS-H6/pET24b	This work

Oligonucleotides used in this study

Number	Name	
oNS024	-	GCCGAATTCGTTTCCACGTTCTGTACTGTG
oNS025	-	GCCGGATCCCAGAGTGGAGGCAAGAACGCC
-	BL1	AGGTCGCCGCCC/3BioTEG/
oTG001F	EcoRI_NheI_F	ACGCTAGCTCTAATAAAAAACAGTCAAATAGGCTAACTG
oTG001R	EcoRI_EcoRI_R	ACGAATTCTCACTTAGATGTAAGCTGTTCAAACAAG
oTG024F	Spo0J_KCK_for	TCTGAACGAGAATCAGGTTCTAAGTGCAAGTAAATGAAAAAACCATC
oTG024R	Spo0J_KCK_rev	GATGGTTTTTTCATTTACTTGCACTTAGAACCTGATTCTCGTTCAGA
oTG025F	Spo0J_deltaC_for	GTTGAATCAGAATGTTCCACGTGAATAAATGAAAAAACCATCTTTCAAACG
oTG025R	Spo0J_deltaC_rev	CGTTTGAAAGATGGTTTTTTCATTTATTCACGTGGAACATTCTGATTCAAC
oTG026F	Spo0J_R149A_for	CGTCTTGGGAAAAGCGCACCGCATATTGCGAA
oTG026R	Spo0J_R149A_rev	TTCGCAATATGCGGTGCGCTTTTCCCAAGACG

oTG027F	Spo0J_R80A_for	GTTGCGGGTGAACGGGCTTTTCGAGCGGCAAAG
oTG027R	Spo0J_R80A_rev	CTTTGCCGCTCGAAAAGCCCGTTCACCCGCAAC
oTG037F	Spo0J_deltaC20_for	AGGCAAAATCGAAATTTAAATGAAAAAACCATC
oTG037R	Spo0J_deltaC20_rev	GATGGTTTTTTCATTTAAATTTCGATTTTGCCT
oTG038F	Spo0J_KCK_deltaC20_for	AGGCAAAATCGAAATTGGTTCTAAGTGCAAG
oTG038R	Spo0J_KCK_deltaC20_rev	CTTGCACTTAGAACCAATTTCGATTTTGCCT
oTG039F	KCK_Spo0J_for	GAGAACAGATTGGTGGTAAGTGCAAGATGGCTAAAGGCCTT
oTG039R	KCK_Spo0J_rev	AAGGCCTTTAGCCATCTTGCACTTACCACCAATCTGTTCTC
oTG041F	parS1_for	CAGTTGAATCAGAATGTTCCACGTGAAACAAAGAAAAAA
oTG041R	parS1_rev	TTTTTTCTTTGTTTCACGTGGAACATTCTGATTCAACTG
oTG043F	parS2_for (scrambled *parS*)	CAGTTGAATCTGACAAATGACTAACAATGAGAGCAAAAA
oTG043R	parS2_rev	TTTTTGCTCTCATTGTTAGTCATTTGTCAGATTCAACTG
oTG039R	KCK_Spo0J_rev	AAGGCCTTTAGCCATCTTGCACTTACCACCAATCTGTTCTC
oTG049F	Spo0J_G77S_for	TATGATATTGTTGCGAGTGAACGGCGTTTTC
oTG049R	Spo0J_G77S_rev	GAAAACGCCGTTCACTCGCAACAATATCATA
oTG122	P1ParB_BamHI_F	AGCTGGATCCATGTCAAAGAAAAACAGACCAACAATTG
oTG123	P1ParB_XhoI_R	AGCTCTCGAGTTAAGGCTTCGGCTTTTTATCGA
oTG133	PaeParB_BamHI_F	AGCTGGATCCATGGCAGCCAAGAAACGTGG
oTG134	PaeParB_SalI_F	AGCTGTCGACTCAACGGATGTGGGCGAGAA
oTG135	SpnParB_BamHI_F	AGCTGGATCCATGGAAAAATTTGAAATGATTTCTATCACAGAT
oTG136	SpnParB_XhoI_R	AGCTCTCGAGTTATTTCAGGCTGTTGATAATTCTACTATATTCT
oTG167	Spo0J_R79A_F	ATTGTTGCGGGTGAAGCGCGTTTTCGAGCGGCA

oTG168	Spo0J_R79A_R	TGCCGCTCGAAAACGCGCTTCACCCGCAACAAT
oTG169	Spo0J_R82A_F	GGTGAACGGCGTTTTGCAGCGGCAAAGCTGGCA
oTG170	Spo0J_R82A_R	TGCCAGCTTTGCCGCTGCAAAACGCCGTTCACC
oTG212	Spo0J_R80K_F	GTTGCGGGTGAACGGAAATTTCGAGCGGCAAAG
oTG224	GC – Spo0J_R80K_F	CTTTGCCGCTCGAAATTTCCGTTCACCCGCAAC
oTG227	DL2B	GGGCGGC/3Dig_N/
oTG247	mGFPmut3-Spo0J-deltaC60_F	AACGTGCCCAGGGAGTAAATGAAGAAACCATC
oTG248	mGFPmut3-Spo0J-deltaC60_R	GATGGTTTCTTCATTTACTCCCTGGGCACGTT
oTG249	mGFPmut3-Spo0J-deltaC20_F	AGGCAAAATCGAAATTTAAATGAAGAAACCATC
oTG250	mGFPmut3-Spo0J-deltaC20_R	GATGGTTTCTTCATTTAAATTTCGATTTTGCCT
oTG251	pelB-soj-spo0J-deltaC20_F	AGGCAAAATCGAAATTTAAATGAAGAAACCA
oTG252	pelB-soj-spo0J-deltaC20_R	TGGTTTCTTCATTTAAATTTCGATTTTGCCT
oTG284	R80K_R82A_F	GTTGCGGGTGAACGGAAGTTTGCAGCGGCAAAGCTGGCA
oTG285	R80K_R82A_R	TGCCAGCTTTGCCGCTGCAAACTTCCGTTCACCCGCAAC
odr665	-	CCGCGCTCTTCCGGTATGGCTAAAGGCCTTGGAAAAGG
odr666	-	CGGCTCGAGACCCGTTGCAAAGGCTCACTG
odr802	-	CCGCGCTCTTCCGGTATGAACAAAACAGAACTTATCAATGC
odr803	-	CGGCTCGAGTTATTTTCCGGCAACTGCGTC
oWX438	-	GACCAGGGAGCACTGGTCAAC
oWX439	-	TCCTTCTGCTCCCTCGCTCAG
oWX507	-	CGTGCTTGAATTTTCAATTATTTCCC
oWX508	-	ACCCGTTGCAAAGGCTCACTGGGCGC
oWX674	-	AAACTCGAGTCCGCCAGATCCTTTGTATAGTTCATCCATGCCATG
oWX706	-	CGCAAGCTTACATAAGGAGGAACTACTATGAGTAAAGGAGAAGAACTTTTCACTGG
oWX886	-	CTGAGCGAGGGAGCAGAAGGATCC

		TTTCCAAGGCCTTTAGCCATTCGCAGC
oWX887	-	GTTGACCAGTGCTCCCTGGTCCGAGAATCATAAATGAAAAAACCATCTTTC
oWX888	-	AGAGGTAAACGTAATGCTCGCAGGCC
oWX1086	-	AAACTCGAGATGGCTAAAGGCCTTGGAAAAGGG
oWX1087	-	AAAGGATCCTTACTTGCACTTAGAACCTGATTCTCGTTCAGACAAAAGCTC
odr790	lambda_kan_parS_F	ACAGCCCGCCGGAACCGGTGGGCTTTTTTGTGGGGTGAATAATCAGAATGTTACACGTGAAACAAAGAAAAAATTCCGGGGATCCGTCGACC
odr792	lambda_kan_R	TACAACGTTTCTGCGGCATATCACAAAACGATTACTCCATAACAGGGACATGTAGGCTGGAGCTGCTTCG
odr793		GCATACCTCAGTGGCGTGGAG
odr794		CCATATTTCATGCGTTCAGTC
odr795		AGCTGGCAATTCCGGTTCGC
oLS015F	HNS_NdeI_for	ACATATGAGCGAAGCACTTAAAATTCTGAAC
oLS015R	HNS_XhoI_rev_v2	GCTCGAGTTGCTTGATCAGGAAATCGTC

All oligonucleotide sequences are given in the 5'-3' direction.

Modifications:

/3Dig_N/ - 3' digoxygenin
/3BioTEG/ - 3' biotin

Supplemental References

Autret S, Nair R, Errington J. 2001. Genetic analysis of the chromosome segregation protein Spo0J of Bacillus subtilis: evidence for separate domains involved in DNA binding and interactions with Soj protein. *Mol Microbiol* **41**: 743–55.

Blainey PC, van Oijen AM, Banerjee A, Verdine GL, Xie XS. 2006. A base-excision DNA-repair protein finds intrahelical lesion bases by fast sliding in contact with DNA. *Proc Natl Acad Sci U S A* **103**: 5752–7.

Breier AM, Grossman AD. 2007. Whole-genome analysis of the chromosome partitioning and sporulation protein Spo0J (ParB) reveals spreading and origin-distal sites on the Bacillus subtilis chromosome. *Mol Microbiol* **64**: 703–18.

Datsenko KA, Wanner BL. 2000. One-step inactivation of chromosomal genes in Escherichia coli K-12 using PCR products. *Proc Natl Acad Sci U S A* **97**: 6640–5.

Doan T, Rudner DZ. 2007. Perturbations to engulfment trigger a degradative response that prevents cell-cell signalling during sporulation in Bacillus subtilis. *Mol Microbiol* **64**: 500–11.

Finkelstein IJ, Visnapuu M-L, Greene EC. 2010. Single-molecule imaging reveals mechanisms of protein disruption by a DNA translocase. *Nature* **468**: 983–7.

Fujita M. 2000. Temporal and selective association of multiple sigma factors with RNA polymerase during sporulation in Bacillus subtilis. *Genes Cells* **5**: 79–88.

Fukushima T, Ishikawa S, Yamamoto H, Ogasawara N, Sekiguchi J. 2003. Transcriptional, functional and cytochemical analyses of the veg gene in Bacillus subtilis. *J Biochem* **133**: 475–83.

Gibson DG, Young L, Chuang R-Y, Venter JC, Hutchison CA, Smith HO. 2009. Enzymatic assembly of DNA molecules up to several hundred kilobases. *Nat Methods* **6**: 343–5.

Ireton K, Gunther NW, Grossman AD. 1994a. spo0J is required for normal chromosome segregation as well as the initiation of sporulation in Bacillus subtilis. *J Bacteriol* **176**: 5320–9.

Ireton K, Gunther NW, Grossman AD. 1994b. spo0J is required for normal chromosome segregation as well as the initiation of sporulation in Bacillus subtilis. *J Bacteriol* **176**: 5320–9.

Landgraf D, Okumus B, Chien P, Baker TA, Paulsson J. 2012. Segregation of molecules at cell division reveals native protein localization. *Nat Methods* **9**: 480–2.

Leonard TA, Butler PJG, Löwe J. 2004. Structural analysis of the chromosome segregation protein Spo0J from Thermus thermophilus. *Mol Microbiol* **53**: 419–32.

Lin DC, Grossman AD. 1998. Identification and characterization of a bacterial chromosome partitioning site. *Cell* **92**: 675–85.

Lin DC, Levin PA, Grossman AD. 1997. Bipolar localization of a chromosome partition protein in Bacillus subtilis. *Proc Natl Acad Sci U S A* **94**: 4721–6.

Murray H, Ferreira H, Errington J. 2006. The bacterial chromosome segregation protein Spo0J spreads along DNA from parS nucleation sites. *Mol Microbiol* **61**: 1352–61.

Van Noort J, Verbrugge S, Goosen N, Dekker C, Dame RT. 2004. Dual architectural roles of HU: formation of flexible hinges and rigid filaments. *Proc Natl Acad Sci U S A* **101**: 6969–74.

Rudner DZ, Fawcett P, Losick R. 1999. A family of membrane-embedded metalloproteases involved in regulated proteolysis of membrane-associated transcription factors. *Proc Natl Acad Sci U S A* **96**: 14765–70.

Sliusarenko O, Heinritz J, Emonet T, Jacobs-Wagner C. 2011. High-throughput, subpixel precision analysis of bacterial morphogenesis and intracellular spatio-temporal dynamics. *Mol Microbiol* **80**: 612–27.

Sullivan NL, Marquis KA, Rudner DZ. 2009. Recruitment of SMC by ParB-parS organizes the origin region and promotes efficient chromosome segregation. *Cell* **137**: 697–707.

Tafvizi A, Huang F, Leith JS, Fersht AR, Mirny LA, van Oijen AM. 2008. Tumor suppressor p53 slides on DNA with low friction and high stability. *Biophys J* **95**: L01–3.

Tanner NA, Hamdan SM, Jergic S, Loscha K V, Schaeffer PM, Dixon NE, van Oijen AM. 2008. Single-molecule studies of fork dynamics in Escherichia coli DNA replication. *Nat Struct Mol Biol* **15**: 998.

Thomason LC, Oppenheim AB, Court DL. 2009. Modifying bacteriophage lambda with recombineering. *Methods Mol Biol* **501**: 239–51.

Wagner-Herman JK, Bernard R, Dunne R, Bisson-Filho AW, Kumar K, Nguyen T, Mulcahy L, Koullias J, Gueiros-Filho FJ, Rudner DZ. 2012. RefZ facilitates the switch from medial to polar division during spore formation in Bacillus subtilis. *J Bacteriol* **194**: 4608–18.

Wang I-N. 2006. Lysis timing and bacteriophage fitness. *Genetics* **172**: 17–26.

Wright DJ, King K, Modrich P. 1989. The negative charge of Glu-111 is required to activate the cleavage center of EcoRI endonuclease. *J Biol Chem* **264**: 11816–21.